J Neurophysiol 92: 3030–3042, 2004.
First published June 16, 2004; 10.1152/jn.00822.2003.

Temporal Dynamics of Shape Analysis in Macaque Visual Area V2

Jay Hegdé and David C. Van Essen
Department of Anatomy and Neurobiology, Washington University School of Medicine, St. Louis, Missouri 63110

Submitted 22 August 2003; accepted in final form 8 June 2004

Hegdé, Jay and David C. Van Essen. Temporal dynamics of shape analysis in macaque visual area V2. *J Neurophysiol* 92: 3030–3042, 2004. First published June 16, 2004; 10.1152/jn.00822.2003. The firing rate of visual cortical neurons typically changes substantially during a sustained visual stimulus. To assess whether, and to what extent, the information about shape conveyed by neurons in visual area V2 changes over the course of the response, we recorded the responses of V2 neurons in awake, fixating monkeys while presenting a diverse set of static shape stimuli within the classical receptive field. We analyzed the time course of various measures of responsiveness and stimulus-related response modulation at the level of individual cells and of the population. For a majority of V2 cells, the response modulation was maximal during the initial transient response (40–80 ms after stimulus onset). During the same period, the population response was relatively correlated, in that V2 cells tended to respond similarly to specific subsets of stimuli. Over the ensuing 80–100 ms, the signal-to-noise ratio of individual cells generally declined, but to a lesser degree than the evoked-response rate during the corresponding time bins, and the response profiles became decorrelated for many individual cells. Concomitantly, the population response became substantially decorrelated. Our results indicate that the information about stimulus shape evolves dynamically and relatively rapidly in V2 during static visual stimulation in ways that may contribute to form discrimination.

INTRODUCTION

Much research in neural information processing is predicated on the notion that neurons convey information by varying their firing rate. According to the rate coding hypothesis (Abbott 1994; Adrian 1926; Rieke et al. 1998), a given visual cortical neuron conveys information about a given set of visual stimuli according to how its average firing rate is modulated across the stimulus set (Pouget et al. 2000; Shadlen and Newsome 1998).

Fluctuations in firing rate can be classified into 2 major types. First, firing rates tend to fluctuate randomly from one presentation to the next of the same stimulus (Shadlen and Newsome 1998; Tolhurst et al. 1983). Trial-to-trial fluctuation of firing rates (noise) and the effects of noise on the information carried by the neuron have been characterized extensively in various areas of the visual system (Abbott 1994; McAdams and Maunsell 1999; Shadlen and Newsome 1994; Wiener et al. 2001; also see Softky and Koch 1993). Second, the firing rate of a visual cortical neuron rarely stays constant during a sustained presentation of a given stimulus; the neuronal response to visual stimulation typically includes an initial transient peak followed by a declining response (Keysers et al. 2001; Lisberger and Movshon 1999; Müller et al. 1999, 2001; Oram and Perrett 1992; Tolhurst et al. 1980, 1983; also see Rieke et al. 1998). Explorations of the effects of this latter type of firing rate variation in the visual cortex have largely focused on the temporal dynamics of selectivity for various low-level stimulus characteristics, such as orientation, spatial frequency, contrast, and disparity, notably in area V1 (see, e.g., Albrecht et al. 2002; Bredfeldt and Ringach 2002; Frazor et al. 2004; Menz and Freeman 2003, 2004; Müller et al. 2001; Shapley et al. 2003; also see DISCUSSION). Additional studies have examined the temporal dynamics of selectivity for orientation contrast in V1 (Knierim and Van Essen 1992), illusory contours in V2 (Lee and Nguyen 2001), "border ownership " in V2 and V4 (Zhou et al. 2000), complex chromatic and achromatic shapes in inferotemporal cortex (Edwards et al. 2003; Keysers et al. 2001; Oram and Perrett 1992; Tovée et al. 1993), and motion-based features in middle temporal (MT), middle superior temporal (MST), and ventral intraparietal (VIP) areas (Cook and Maunsell 2002; Duffy and Wurtz 1997; Pack and Born 2001; also see DISCUSSION). However, neither the temporal dynamics of intermediate level shape processing nor the interplay between temporal dynamics and signal-to-noise have been systematically studied in the extrastriate cortex.

Here, we examine the temporal dynamics of the response to shape stimuli of low- to intermediate complexity in the extrastriate visual area V2. We previously showed that neurons in V2 carry detailed shape information about a diverse set of visual shapes, including a variety of gratings and contours (Hegdé and Van Essen 2000, 2003). Using this data set, we studied the temporal dynamics of 3 main types of firing rate variation in V2: *1*) stimulus-to-stimulus variation, or signal; *2*) trial-to-trial variation, or noise; and *3*) cell-to-cell variation in the response to a given stimulus. Our study addressed the temporal dynamics of the shape information conveyed by the firing rate and not the information conveyed by the temporal pattern the responses per se (McClurkin et al. 1991; Richmond and Optican 1990), or by synchronized firing among subsets of neurons (see Gray 1999; Salinas and Sejnowski 2001; Usrey and Reid 1999).

We find that the magnitude and the nature of the information carried by individual neurons and by the V2 cell population change substantially over the course of the response. The maximal response modulation at the individual cell level occurs during the initial response transients. Information about shape decorrelates over time for many individual cells and for the population, suggesting that shape representation in V2 changes in meaningful ways in association with temporal variations in the firing rate.

Address for reprint requests and other correspondence: D. Van Essen, Department of Anatomy and Neurobiology, Box 8108, Washington University School of Medicine, St. Louis, MO 63110 (E-mail: vanessen@brainvis.wustl.edu).

The costs of publication of this article were defrayed in part by the payment of page charges. The article must therefore be hereby marked "*advertisement*" in accordance with 18 U.S.C. Section 1734 solely to indicate this fact.

METHODS

The responses of single units to shape stimuli were recorded in area V2 of awake, fixating monkeys, using experimental procedures described elsewhere (Hegdé and Van Essen 2000, 2003). Briefly, 3 adult male macaques (2 *Macaca mulatta* and one *Macaca fascicularis*) were used in this study. Each animal was implanted with a scleral search coil and an acrylic cranial patch using sterile surgical procedures. After a given animal was fully trained in the fixation task, a small craniotomy 5 mm in diameter was made over the recording site, and a recording chamber was mounted over the craniotomy. Neurophysiological recording was carried out using epoxy-coated tungsten electrodes (A-M Systems, Carlsborg, WA) with initial impedances of 3–5 MΩ (at 1 kHz) inserted transdurally into the cortex. All animal-related procedures used in this study were reviewed and approved in advance by the Washington University Animal Studies Committee.

Visual stimulation and recording

The animal fixated within a fixation window of 0.5° radius for a juice reward while stimuli were presented within the classical receptive field of the V2 cell under study. The stimulus set consisted of 48 grating stimuli and 80 contour stimuli (Fig. 1). Grating stimuli consisted of conventional sinusoidal gratings, as well as non-Cartesian (hyperbolic and polar) gratings. The contour stimuli consisted of bars, intersections (tristars, crosses, and 5- and 6-armed stars), angles (acute angles, right angles, and obtuse angles), arcs (one-quarter arcs, semicircles, and three-quarter arcs), and circles. The large contour stimuli were matched in size to the cell's preferred bar length (determined qualitatively during receptive field mapping), with the exception of larger obtuse angles and one-quarter arcs, which were scaled down 50% to ensure that they stayed within the classical receptive field. The smaller contours in all cases were one half the size of the corresponding larger contours.

The rationale for the stimulus set has been described previously (Hegdé and Van Essen 2000, 2003). Briefly, the stimuli were selected to probe the selectivity of V2 cells for a variety of low- and intermediate-level form cues. The grating stimuli probe the selectivity for conventional spatial frequency and orientation (sinusoids), as well as more complex textural characteristics (non-Cartesian gratings), which the visual system may use as basis functions for surface representation (Eagleson 1992; Perona 1991; Wilkinson et al. 1998; also see Bergen 1991; Gallant et al. 1996). The contour stimuli probe the selectivity for conventional orientation (bar stimuli), along with selectivity for the angles, intersections, orientations, and curvature of visual contours, which may play an important role in image segmentation and object recognition (Geisler and Super 2000; Geisler et al. 2001; Rogers-Ramachandran and Ramachandran 1997; Sigman et al. 2001). Although our stimuli explored a relatively large stimulus space, they did not address many other important shape cues (e.g., disparity, motion, etc.), and sampled many important shape characteristics (e.g., curvature) only sparsely because of practical limitations on the size of the stimulus set.

Single cells were isolated using a window discriminator (Bak Electronics, Germantown, MD). The cell's receptive field was mapped using multiple mouse-driven bar- or grating stimuli on the computer's monitor. The cell's preferred bar parameters, including preferred length, width, color, and orientation, were also determined during the manual mapping. For the recording, the stimulus set was reoriented for each cell according to the cell's preferred orientation (also see legend to Fig. 1). All stimuli were presented in the cell's preferred color (qualitatively assessed using a palette of 6 colors) over a uniform gray background. The line width of contour stimuli was determined by cell's qualitatively estimated preferred bar width. The grating stimuli had a spatial frequency of 2, 4, or 6 cycles per receptive field diameter and had the same diameter as that of the receptive field and the same mean luminance as that of the background. Stimuli were presented sequentially for 300 ms each with a 300 ms interstimulus interval. Up to 6 stimuli were presented per trial in this fashion. The stimuli were randomly interleaved, so that the effects of systematic eye position drifts, and so forth, over the course of the trial were minimized. In general, the fixation jitter was much narrower for each of the 3 animals than the ±0.5° range allowed, and none of the animals showed any drifts or other systematic effects of fixation fatigue. To reduce the contributions of any receptive field nonuniformities, each stimulus was presented at 3 different jitter positions, spaced evenly from each other, and offset from the receptive field center by 25% of the receptive field radius.

The spikes were collected at a resolution of 1 ms using a Silicon Graphics Indigo2 workstation using custom-written experimental control software. Presentation of visual stimuli was synchronized with the spike-collection software at a temporal resolution of ±7 ms (i.e., 1/72 Hz, the screen refresh rate). The response to each stimulus was recorded over 12 randomly interleaved repetitions (except for 62 cells from one animal, which had 9 repetitions per stimulus, 3 at each jitter position). Only the data from trials throughout which the animal maintained fixation were further analyzed.

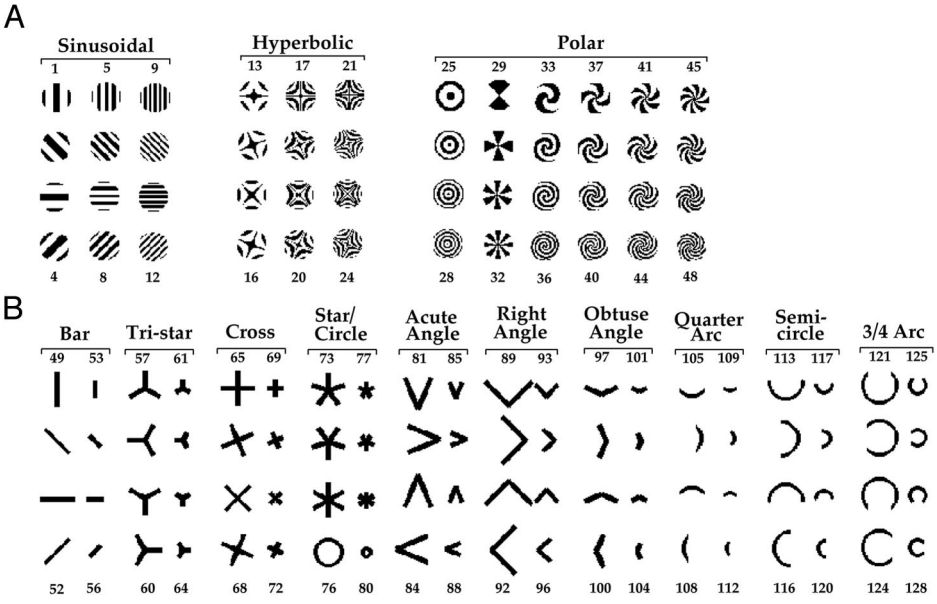

FIG. 1. Stimulus set, consisting of 128 stimuli, 48 of which were gratings and 80 were contour stimuli. *A*: grating stimuli included 12 sinusoidal gratings, 12 hyperbolic gratings, and 24 polar gratings. *B*: 80 contour stimuli included bars, tristars, crosses, stars, acute angles, right angles, obtuse angles, one-quarter arcs, semicircles, and three-quarter arcs and circles. For the purposes of many of the analyses in this study, the stimuli were numbered sequentially from 1 through 128 (grating stimuli from 1 through 48, and the contour stimuli from 49 through 128) as indicated by the *numbers* above and below each column of stimuli.

Data analyses

The data were analyzed using the statistical utility S-Plus (Insightful, Seattle, WA) or Matlab (The Mathworks, Natick, MA) or custom-written C language software. A total of 196 cells were recorded from 4 hemispheres of 3 animals. In 180 cells, at least one of the 128 stimuli evoked a response greater than the background at a significance level of $P < 0.05$ (2-tailed *t*-test with Bonferroni correction for 128 comparisons, $\alpha = 0.05/128$; see Huberty and Morris 1989; also see Savitz and Olshan 1995; Thompson 1998); all 180 of these were included in this study.

ASSIGNING SPIKES INTO BINS. Spikes fired by the given cell between 0 and 300 ms after stimulus onset were analyzed in this study, unless specified otherwise. For most analyses, the spikes in response to each presentation of each stimulus were divided into 15 consecutive time bins of 20 ms, each extending from 0–300 ms, so that the bins had identical binwidth but contained a variable number of spikes, depending on the cell's firing rate during the given bin. For some analyses, 15 consecutive bins that contained equal number of spikes but had variable binwidth were used instead. To calculate these bins for a given cell, the spikes fired by the cell across all repetitions of all stimuli were pooled, preserving the relative temporal order in which they occurred during the 0–300 ms time interval. This ordered train of spikes was divided into 15 consecutive bins so that each bin contained an equal number of spikes; the final 14 or fewer spikes closest to the 300 ms mark were discarded so as to avoid fractional spike counts.

TESTS OF SIGNIFICANCE. Conventional parametric tests of significance were used where appropriate. In most cases, however, we used randomization analysis, by determining whether the value of a suitable test statistic calculated from the actual data differs significantly from the distribution of the same test statistic calculated from randomized data (see Edgington 1995; Manly 1991). For each test, an appropriate test statistic was first calculated using the actual neural response data. The data were then randomized across bins, trials, stimuli, and/or cells as appropriate, and the test statistic was recalculated using the randomized data. The randomization process was repeated 10^6 times [10^3 times in the case of multidimensional scaling (MDS) analyses described below]. The proportion of times the randomized test statistic exceeded the actual test statistic constituted the one-tailed probability *P* that the actual value of the test statistic was attributed to chance.

In cases involving multiple comparisons, we adopted a stringent approach of using the Bonferroni correction ($\alpha = 0.05/n$, where α is the probability of type I error and *n* is the number of comparisons; see Huberty and Morris 1989; also see Savitz and Olshan 1995; Thompson 1998).

INDICES. To measure the sharpness of a given cell's shape selectivity profile during a given bin, we used the *tuning sharpness index* (TSI), defined as $[1 - (R_{mean}/R_{max})]$, where R_{mean} is the cell's mean response to all 128 stimuli and R_{max} is the cell's response to its most effective stimulus. The TSI is sensitive to noise, given that random fluctuations in firing rate will tend to increase R_{max} by chance without affecting R_{mean}, thus increasing TSI.

To measure the modulation of a given cell's responses above random noise levels by the stimuli, we used the *response modulation index* (RMI). To calculate RMI for a given cell during a given bin, we first calculated the conventional *F* ratio of the cell's responses to the given set of stimuli, given by $F = MS_{between}/MS_{within}$, where $MS_{between}$ is the stimulus-to-stimulus variance across trials (or, equivalently, the between-stimulus mean squares), and the MS_{within} is the average trial-to-trial variance. The *F* ratio is an explicit measure of the signal-to-noise ratio because $MS_{between}$ and MS_{within} are measures of the signal and the noise, respectively. Note that $MS_{between}$ values subsume the corresponding MS_{within} values, so that $MS_{between}$ represents both the stimulus-to-stimulus variance and trial-to-trial variance, whereas MS_{within} represents only the trial-to-trial variance (see Brase and Brase 1995). To calculate RMI, we randomized the responses across the stimuli and recalculated the *F* ratio. RMI was defined as the *F* ratio calculated from the actual data divided by the average *F* ratio from the randomization rounds. This normalization of the actual *F* ratio with the average randomized *F* ratio effectively corrected for deviations of the data set from normality. We did not use information-theoretic measures to quantify information, mainly because the number of repetitions per stimulus in our data set (9–12 depending on the cell) was too small for such analyses. Briefly, small sample sizes (i.e., small number of repetitions) result in systematic biases in the information-theoretic estimates of the information conveyed (Panzeri 1996; Panzeri and Treves 1996). To correct for these biases is desirable to have at least as many repetitions per stimuli as there are stimuli in the stimuli set (128 in our case); smaller number of repetitions will result in systematic *overestimation* of the information conveyed (Panzeri 1996, p. 91–94; Panzeri and Treves 1996, p. 90–100; also see Rolls et al. 2003). Note that ad hoc corrections, including those suggested by Chee-Orts and Optican (1993), do not adequately correct for this error (see Panzeri 1996, p. 91–94; Panzeri and Treves 1996, p. 88).

CALCULATING POPULATION AVERAGES. To calculate the population average of a given metric, we first normalized the values of the metric across all time bins to a maximum of 1.0 for each cell to correct for cell-to-cell differences in the response magnitude. We then averaged the normalized values across all 180 cells separately for each bin. SE values were calculated for each bin as the SE of the normalized values across all cells in that bin. The only exception to this procedure was the population average of the sharpness of tuning index (TSI) values shown in Fig. 4*D*, which were averaged across the population without being normalized, because the TSI values ranged from 0 to 1 to begin with.

CALCULATING THE TIME OF MAXIMUM RESPONSE AND MAXIMUM RESPONSE MODULATION. For each cell, the time histograms of the firing rate and of the RMI across the 15 bins were smoothed separately using a Gaussian filter ($\sigma = 10$ ms), and the time value corresponding to the peak was determined to the nearest millisecond. We used randomization analysis (see above) to determine whether the peaks were the result of noise. To do this for the RMI peak for a given cell, we randomized the spike counts of the cell across all bins and stimuli and recalculated the RMI for each bin. We then smoothed the resulting 15-bin time histogram and determined the peak as for the nonrandomized data. This procedure was repeated for 1,000 rounds. The proportion of rounds during which the peak was at least as tall as the peak from that from the actual data represented the one-tailed probability *P* that the peak from the actual data was attributed to noise. The statistical significance of the firing rate peaks was determined similarly.

Analysis of response correlations at the population level

To analyze patterns of response correlation across the population, we used metric MDS and principal components analysis (PCA), as described in Hegdé and Van Essen (2003). Briefly, we used a 128 × 128 correlation matrix of the population response as the input to MDS or PCA. Each element of the matrix represented the correlation coefficient of the responses of the V2 cells (averaged across trials, but non-normalized) to a given pair of the 128 stimuli (see Fig. 8*A*; also see Hegdé and Van Essen 2003; Kachigan 1991, p. 147).

We used MDS (S-Plus routine *cmdscale*; for an overview, see Kachigan 1991) to visualize the large patterns of correlation in the population response to the various stimuli, so that the distances between the stimuli represents the similarity of the responses of V2 cells to the stimuli. The MDS algorithm begins with an arbitrary placement of the stimuli and iteratively shifts the stimuli to reduce the distortion (or "stress") between the interstimulus distances and the

original similarities. Some stress is inevitable when reducing high-dimensional data into a 2-dimensional format, given that interstimulus distances can rarely be found in a 2-dimensional plot that exactly match the similarities in a 128 × 128 dimensional matrix. However, the algorithm finds the best representation of similarities with the least amount of distortion, so that stimuli that elicit dissimilar responses are dispersed from each other and the stimuli that elicit similar responses are clustered together.

ANALYSIS OF MDS CLUSTERS: *D* RATIO TEST. We used randomization analysis to determine whether the clustering of stimuli, if any, in a given MDS plot was significantly nonrandom. The test statistic was the *D* ratio, which was directly analogous to the conventional *F* ratio, making the *D* ratio test a direct analog of the *F* test. An MDS plot was first generated using the original 128 × 128 correlation matrix described above. Clusters of data points were provisionally identified from a visual examination of the plot and used to calculate the *D* ratio, defined as the variance of the between-cluster distances divided by the mean variance of within-cluster distances. The correlation matrix was then randomized and an MDS plot was generated from the randomized matrix. The *D* ratio was calculated for this MDS plot using the original composition of the clusters. The clustering in the original matrix was considered significantly nonrandom if the *P* value was <0.05.

COPHENETIC CORRELATION. Cophenetic correlation is a method of calculating the correlation coefficient between paired matrices or other high-dimensional data (for overviews, see Sneath and Sokal 1973; Sokal and Rohlf 1962). We used a version of this method to measure the similarity between a given pair of MDS plots or correlation matrices (for details, see Hegdé and Van Essen 2003). Like the conventional correlation coefficient, the values of r_C vary from 1.0 (perfect correlation) to 0.0 (no correlation) to −1.0 (perfect anticorrelation).

PCA (S-Plus routine *princomp*) simplifies complex, high-dimensional data by identifying a small number factors that underlie global patterns in the data and determining the extent to which each factor, or principal component, accounts for variance in the data. In a manner analogous, but not identical, to multiple linear regression, PCA linearly transforms an original set of variables into a smaller set of independent (uncorrelated) variables (principal components) that represent most of the information in the original set of variables. If the given data set is highly correlated (or equivalently, redundant or low-dimensional), a small number of principal components will account for a large proportion of the data, and the proportion of data explained will tend to fall off sharply from the top component on. As the input data become increasingly decorrelated (or increase in dimensionality, or decrease in redundancy) it takes progressively more principal components to account for a given proportion of the data, and successive principal components will tend to account for more comparable proportions of data. We used this technique to assess the temporal variations in the dimensionality of the V2 population response.

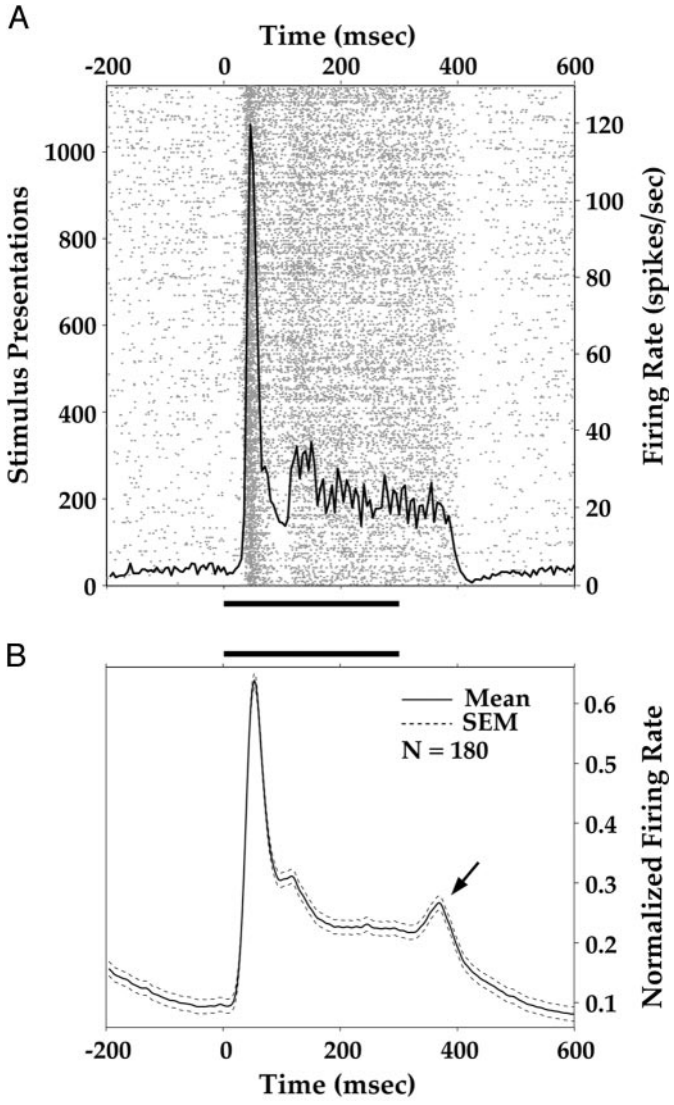

FIG. 2. Temporal dynamics of the firing rates. *A*: response rasters of an exemplar V2 cell. During each trial, up to 6 stimuli were presented one after another for 300 ms each (thick horizontal bar) with 300-ms interstimulus interval, while the animal maintained fixation (see METHODS). Here, the data from each trial are parsed according to the stimuli, so that the spikes (dots) occurring before, during, and after the presentation of a single stimulus are shown on a raster line of its own. Rasters are arranged in the order in which the stimuli were presented to the cell, starting with the earliest at the *bottom*, and are vertically aligned with respect to the stimulus onset. *Solid trace* denotes the aggregate poststimulus time histogram of the cell's responses across all presentations of all stimuli (bin size, 5 ms). Firing rate remained significantly above background levels throughout the cell's response (binwise one-tailed *t*-test, $P < 0.05$; binwidth, 5 ms). *B*: population average. Solid line and the dotted lines denote population average ± SE (see METHODS). Arrow points to the OFF-response. Note that the responses to visual stimulation persist into, and gradually decline during, the early part of the subsequent interstimulus interval.

RESULTS

Temporal dynamics of the firing rates

When tested with the stimulus set shown in Fig. 1, many V2 cells responded with a brisk initial transient response that rapidly decayed to a sustained level at a lower firing rate. In Fig. 2*A*, the response pattern for an exemplar V2 cell is shown as the average firing rate across all stimulus presentations, superimposed on individual raster patterns that are ordered in the actual sequence of stimulus presentation. The cell had low spontaneous activity (4 spikes/s), responded with a latency of about 30 ms after stimulus onset, fired maximally (121 spikes/s) about 50 ms after stimulus onset, declined rapidly to below 20 spikes/s, then rebounded to a sustained rate of 20–30 spikes/s. The average response for the entire population of V2 cells (Fig. 2*B*, solid line), showed a similar response pattern, including a rapid transient response (35–85 ms after the stimulus onset), a sustained response at about 40% of the peak rate, and a modest OFF-response (arrow).

Stimulus-to-stimulus differences in the temporal dynamics of the firing rate

Figure 3 illustrates the spike density function (SDF) for individual stimuli presented to the exemplar cell, with each row showing the SDF for a single stimulus averaged across 9 repetitions. Numerous stimuli elicited strong responses during the 40–60 ms interval after the stimulus onset, but most of those were far less effective later in the stimulation period. In contrast, a few stimuli including the large acute angles at 0 and 180° (*rows 81* and *83*), elicited a relatively strong response throughout the stimulus presentation.

To analyze how the exemplar cell's shape selectivity profile (i.e., the responses of the cell to all 128 stimuli) varied with time, we divided the responses of the cell during the 300-ms visual stimulation into consecutive 20 ms bins and determined the cell's response profile during each bin. Figure 4*A* shows the cell's response profile during the 40–60 ms time window, using a display in which each stimulus is colored according to the mean response it elicited during this window. During this window, which included the initial response peak, the cell responded maximally to an intermediate frequency radial grating (187 spikes/s, *third row*) and also relatively well to a variety of other gratings, intersections, and angles. The sharpness of the cell's selectivity, measured using the TSI (see METHODS), was 0.59 during this bin (thin red line in Fig. 4*D*), corresponding to a 2.4-fold ratio between the most effective stimulus and the average response to all 128 stimuli during this time window.

During the 160–180 ms time window (Fig. 4*B*), the most effective stimuli were the large acute angles at 180° (122 spikes/s, *third row*) and 0° (120 spikes/s, *first row*). The cell responded poorly to most other stimuli, including many that were effective during the 40–60 ms bin (e.g., the intermediate frequency radial grating, *third row*). The TSI increased to 0.8 for the 60–80 ms window, corresponding to a 5-fold ratio between the best and the average response, and it remained near this level for the remainder of the stimulus presentation (Fig. 4*D*, thin red line). Overall, the cell's shape-selectivity profiles during the 40–60 ms bin versus the 160–180 ms bin were poorly correlated (correlation coefficient $r = 0.17$). The shape-selectivity profile calculated over the entire 300 ms interval (Fig. 4*C*) largely resembled that during the 160–180 ms bin ($r = 0.69$), indicating that there was reasonable consistency in shape selectivity after the initial transient. Together, these results indicate that the response profile of the exemplar cell substantially decorrelated over the course of the response.

The broader tuning (i.e., decreased TSI) during initial transients might in principle reflect a saturation effect, in which many stimuli elicit a near-maximal firing rate. If saturation occurred and were related to the cell's relative refractory period, the variance/mean ratio (VMR) of the responses across all stimuli should decrease during the initial transient, as indeed occurs in V1 cells responding to flashed gratings (Mül-

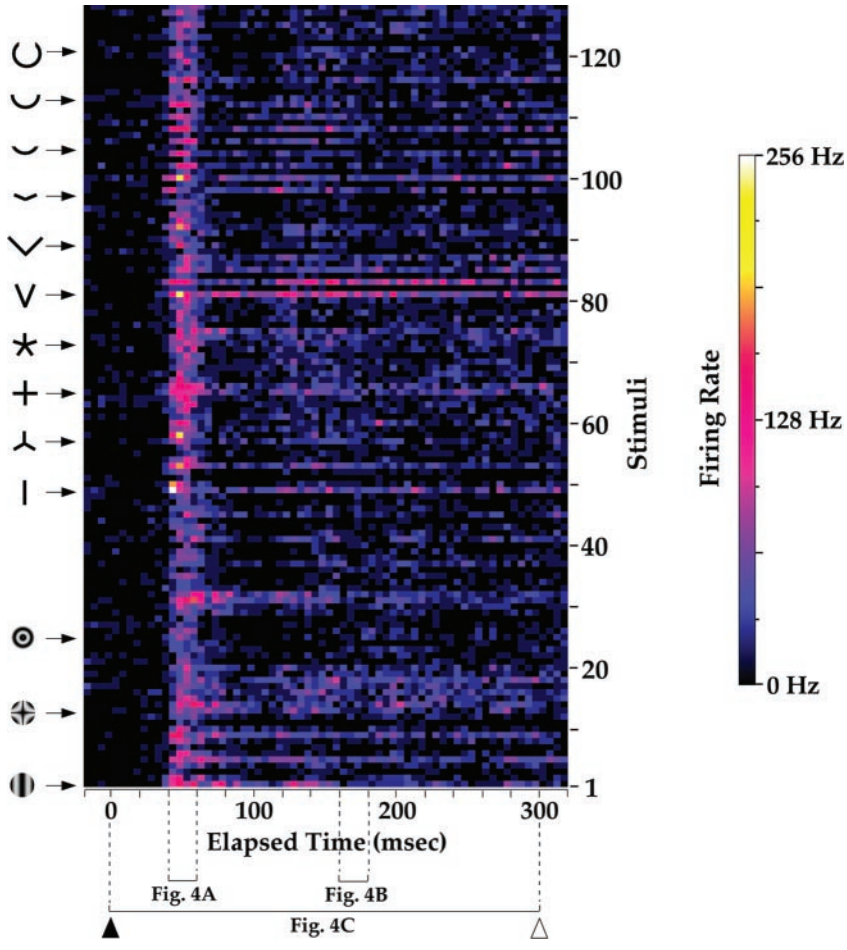

FIG. 3. Time course of the response of the exemplar cell to individual stimuli. *Each row* represents the spike density function (SDF) of a single stimulus, drawn according to the color scale shown on the *right*. SDFs in this figure are numbered (*right*) in the same order as the stimuli in Fig. 1; SDFs of representative stimuli from each stimulus subclass are highlighted by the corresponding *icons* on the *left*. Each bin of a given SDF represents the firing rate of the cell during a given 5 ms interval averaged across 9 repetitions of the given stimulus. In this and the subsequent figures, the stimulus onset and offset are denoted by the filled and open arrowheads, respectively. The square brackets at the *bottom* designate the time windows from which the shape selectivity profiles shown in Fig. 4, *A–C* were calculated. For the purposes of many of the analyses in this report, the spikes fired during the 300 ms stimulus presentation were classified into 15 consecutive bins of 20 ms each (*bottom*).

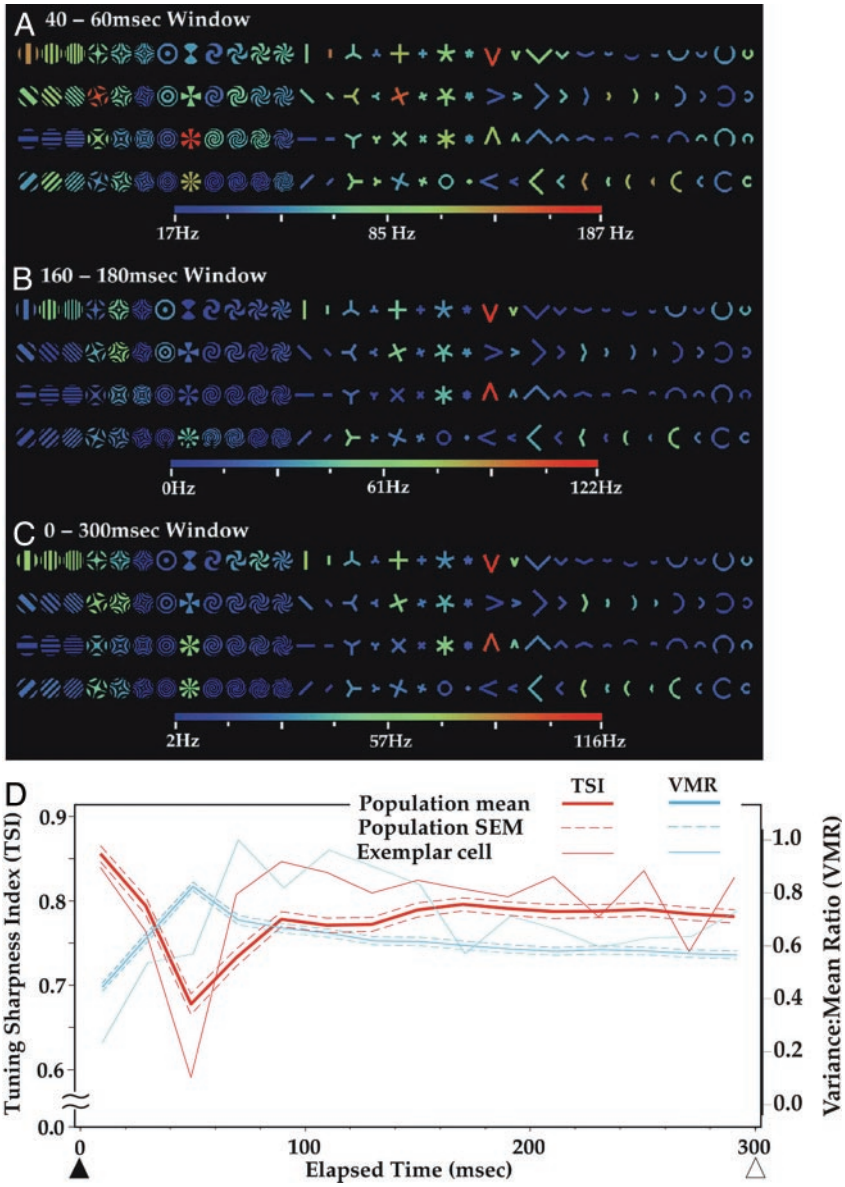

FIG. 4. Shape-selectivity profile of the exemplar cell during different time periods. Response profile of the exemplar cell during 40–60 ms (*A*), 160–180 ms (*B*), or 0–300 ms (*C*) after the stimulus onset are shown. Note that the color scales in the 3 panels are different from each other and from that in Fig. 3. *D*: temporal dynamics of sharpness of shape selectivity. Sharpness of the response profile was measured using the tuning sharpness index (TSI) for each cell during each 20-ms bin. TSI values vary from 0 to 1, with larger values denoting correspondingly sharper tuning (see METHODS). Thin red line denotes the TSI values of the exemplar cell. Thick red line represents the average TSI for all 180 V2 cells; the red dashed lines represent ± SE. Similarly, the thin blue line represents the variance/mean ratio (VMR) values of the exemplar cell, normalized to a maximum of 1.0. Thick blue line and the blue dashed lines represent the population average and ± SE, respectively, of VMR values. In this and the subsequent figures, the data for each 20 ms bin are plotted at the midpoint of the bin.

ler et al. 2001). The VMR computed for the exemplar cell was 0.55 for the 40–60 ms window, increased to about 0.8 in the 60–140 ms window, then declined to about 0.65 after 160 ms. This is consistent with some initial saturation in the exemplar cell. However, for the population response, the VMR (thick blue line) was maximal during the 40–60 ms bin during which TSI was lowest and declined subsequently as the TSI values (thick red line) increased. Thus response saturation related to refractoriness is unlikely to be a general explanation for the increases in tuning sharpness after the initial transient.

Temporal dynamics of the signal-to-noise ratio

To measure the information conveyed by each neuron after accounting for trial-to-trial fluctuations (i.e., noise), we used the response modulation index (RMI), which is based on the *F* ratio and provides an explicit measure of the signal-to-noise ratio (see METHODS). In one analysis, the time course of the RMI was calculated using 20 equal time bins (15 ms/bin). Because the use of equal binwidth could in principle underestimate the response modulation during intervals of low average responses, we carried out a separate analysis in which the bins for each cell were adjusted to give an equal total spike count (see METHODS). The results for both analyses were very similar and are illustrated here only for the equal time bin analysis.

Figure 5*A* shows results for the exemplar cell, with the RMI indicated by the thick solid line and large dots. Measures contributing to the RMI, the conventional *F* ratio (i.e., the signal-to-noise ratio, medium dotted line), and randomized average *F* ratio (thin dashed line), are also shown (see legend for details). The RMI had values of 2.8 and 2.9 during the first 2 responsive bins (20–40 and 40–60 ms), rose to a peak of 6.0 during the 60–80 ms bin, then decreased to about 5 from 100–180 ms and about 3.5 from 180–300 ms. Thus the responses of this cell conveyed significant shape information with a time course that differed substantially from the cell's mean firing rate.

For the population as a whole, the normalized RMI values showed a similar temporal pattern to that of the exemplar cell

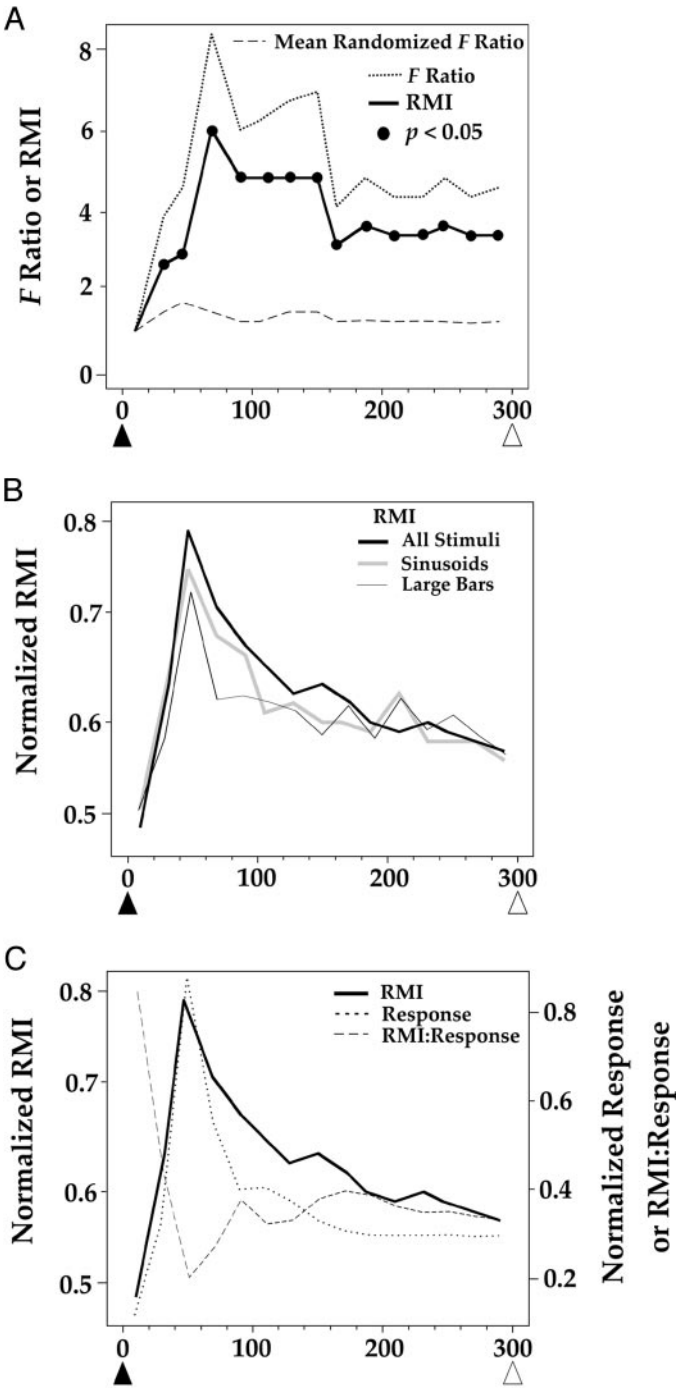

FIG. 5. Temporal dynamics of response modulation. *A*: calculation of the response modulation index (RMI) illustrated using the data for the exemplar cell in Fig. 2. An *F* ratio was calculated during each of the 15 bins. RMI for the given bin was calculated as the actual *F* ratio divided by the average randomized *F* ratio. *B*: population average, calculated by normalizing the RMI values for each cell to a maximum of 1.0 and averaging the normalized values across all cells. Average RMI values calculated using the responses to all 128 stimuli, only to the 12 sinusoids, or only to the 4 large bars are shown. *C*: comparison of response vs. response modulation. Ratio between the firing rate and RMI was calculated for every cell, and the resulting values were normalized to a maximum of 1.0 for each cell and averaged across all cells. Population averages of the RMI:response ratios and the firing rate are drawn to the *y*-scale on the *right*, and the population average of RMI is drawn to the *y*-scale on the *left*. In *C*, the RMI:response ratios are not directly comparable to RMI or firing rate values because they were normalized separately for each cell.

(thick solid line in Fig. 5*B*). The population average RMI peaked during the 40–60 ms bin, and decreased gradually through the remainder of the stimulation period. Direct comparison of the normalized RMI to the normalized mean firing rate (Fig. 5*C*) shows that the RMI declined more slowly than the mean firing rate, resulting in an RMI:response ratio that increased in the interval between 60 and 100 ms.

To assess whether the temporal dynamics depend strongly on the different stimulus classes within our overall stimulus set, we carried out the same analyses, but using the responses to only the 12 sinusoidal stimuli (medium gray line in Fig. 5*B*) or only the 4 oriented bars (thin black line). The results were statistically indistinguishable (one-way ANOVA, $P > 0.05$) for both the exemplar cell (data not shown) and for the population as a whole (Fig. 5*B*), indicating that the information conveyed about spatial frequency and/or orientation follows a similar temporal dynamic pattern as that about the stimulus set as a whole.

Reliability of response modulation during various phases of the response

The population averages of RMI, though informative, do not address the question of whether or to what extent the response modulation was statistically significant during various bins. To address this issue, we determined, for each bin, the cells for which the evoked responses were both significantly above background (as measured by a 2-tailed *t*-test, $P < 0.05$ with Bonferroni correction) and were modulated significantly above random levels (as measured by the RMI, $P < 0.05$ with Bonferroni correction) during the same bin. Of the 180 cells, 161 cells (89%) met both criteria for at least one bin. For each of these 161 cells, we determined the bin during which the cell conveyed the earliest, largest, and latest significant shape information by the above 2 criteria, as illustrated schematically in Fig. 6*A*. The results are shown in Fig. 6, *B–D*. About one third (58/161, 36%) and eight tenths (127/161, 79%) of the cells conveyed significant shape information within 40 and 60 ms of the stimulus onset, respectively (Fig. 6*B*). About one half (81/161, 50%) and two thirds (113/161, 70%) of the cells, respectively, conveyed maximal shape information within the first 60 and 80 ms after the stimulus onset, respectively (Fig. 6*C*). About three tenths of the cells (48/161, 30%) conveyed significant shape information as late as the last (i.e., 280–300 ms) bin, although at lower RMI values (Fig. 6*D*).

Taken together, these results indicate that *1*) the responses of V2 cells tend to be modulated to the greatest extent early on during the response, both in terms of the reliability (i.e., statistical significance) and the magnitude of the response modulation; and *2*) many V2 cells continue to convey significant shape information throughout the response.

Because the modulation of a cell's response is closely related to its firing rate, we investigated whether and to what extent the 2 parameters were correlated for a given cell. To address this issue, we carried out 2 analyses. First, we compared the time of maximal response with the time of maximal response modulation for each cell (Fig. 7*A*). For 151 (84%) of the 180 cells (denoted by filled circles in the scatter plot), the peak response and peak response modulation were both significantly higher than expected from chance, as determined by randomization ($P < 0.05$ with Bonferroni correction; see

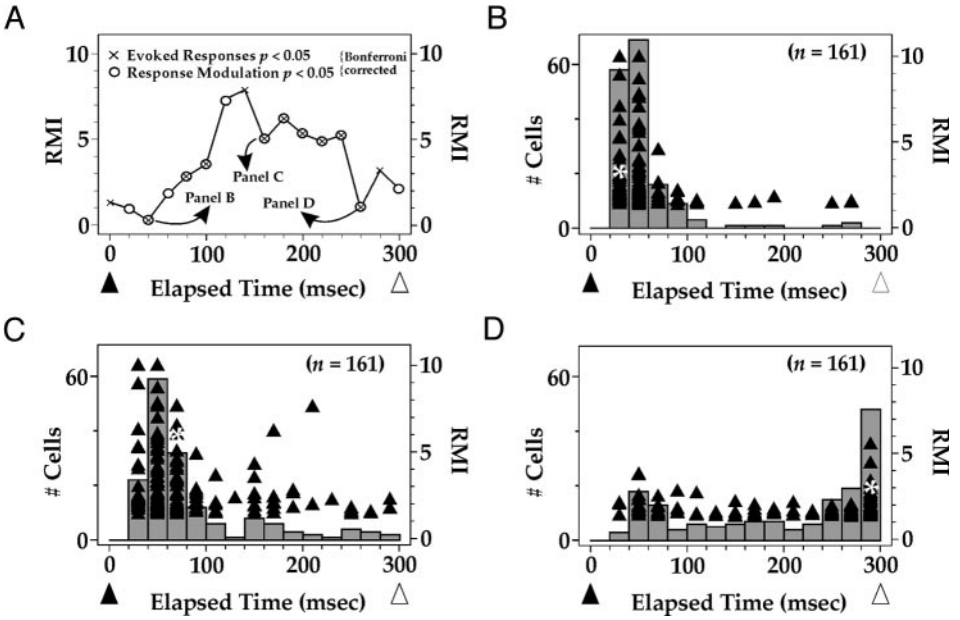

FIG. 6. Magnitude and reliability of response modulation at various stages of the response. Bins during which the evoked responses were both significantly higher than the background levels and significantly modulated across stimuli were determined for each cell, as illustrated schematically in *A* for a hypothetical cell. From the bins that met both of the criteria (⊗ symbols), the earliest bin, the latest bin, and the bin with the largest RMI value were selected for each cell. *B–D*: population distribution of these bins (*B*, earliest bins; *C*, bins with largest RMI values; *D*, the latest bins; all drawn to the same scale to facilitate comparison). In each case, the gray bars in the background show the distribution of the cells across the bins in time-histogram form (*right y*-axis) and the filled triangles denote the actual RMI values of individual cells in each bin (*left y*-axis). Asterisk denotes the exemplar cell in Fig. 2. RMI values >10 were rounded out to 10 in all 3 panels. See RESULTS for details.

METHODS). For these cells and for V2 cells in general, the peak in response modulation was substantially delayed relative to the initial response transients, to an even greater degree than for the exemplar cell. For 30% of the overall population (54/180) and of the cells denoted by filled circles (46/151), the response modulation peaked more than 20 ms after the peak in firing rate. For 23 of these 46 cells (50%), and for 21% of the overall population (37/180), the response modulation (as measured by the RMI value) was significantly larger ($P < 0.05$ with Bonferroni correction) for the bin during which the RMI was maximal than for the bin during which the firing rate was maximal. The overall correlation between peak response and maximum response modulation was poor across all V2 cells ($r = 0.19$), and across the 151 cells with significant peaks in the response and the response modulation ($r = 0.10$). In the second analysis, we calculated the *r* value between RMI and average neuronal response across all bins for each cell. The *r* values varied considerably from one cell to the next (Fig. 7*B*). The correlation was statistically insignificant ($P > 0.05$, $r < 0.58$, one-tailed Pearson product moment correlation) for about three fifths of the cells (105/180, 58%; open bars). The average *r* value for all V2 cells was 0.38. Thus the mean response was a poor predictor of response modulation for many V2 cells.

Temporal changes in the population response

The results presented thus far deal with the temporal dynamics of response modulation at the level of individual cells. We also studied the temporal dynamics of the population response, specifically to determine whether and to what extent the population response decorrelated over time. To do this, we calculated a correlation matrix of the population response during each 20 ms bin, so that each element of a given matrix represented the correlation coefficient *r* between the responses of all V2 cells to a given pair of stimuli (see Fig. 8*A* and METHODS). The matrices corresponding to 4 selected bins are shown in Fig. 8*B*.

The matrices varied significantly across the bins (one-way ANOVA, $P < 0.05$, data not shown). Figure 8*C* shows the mean *r* value (±SE) from the correlation matrix corresponding to each bin. During the first bin (0–20 ms) (i.e., before the response onset), the mean *r* value was low (0.23), and the *r* values were distributed across stimuli apparently randomly (Fig. 8*B*, *panel 1*). The mean *r* values increased sharply over the next 2 bins, peaking at 0.4 during the 40–60 ms bin, when the population average response was maximal (cf. Fig. 2*B*).

The population response decorrelated progressively from 60 to 160 ms, then stabilized at a low level (0.19–0.22) comparable to that of the 0- to 20-ms bin. The SE of the *r* values (error bars in Fig. 8*C*) varied little across all 15 bins (range, 0.009–0.01), even as the mean *r* values varied from one bin to the next, indicating the *r* values rose or fell consistently across the various stimuli from one bin to the next.

During the 40–60 ms bin, the response correlation was highest among the gratings (Fig. 8*B*, *panel 2*, *stimuli 1–48*) and some large contour stimuli. This pattern of correlations is more clearly visualized by the MDS plot of this correlation matrix (Fig. 8*D*), in which the stimuli that elicited relatively consistent responses across the population (i.e., elements of the correlation matrix with similar colors) are clustered together, whereas stimuli that elicited disparate responses from one cell to the next are dispersed farther apart (see METHODS for details). If the response correlations vary randomly among stimuli, the stimuli are expected to scatter randomly, with no significant clustering. If the responses were perfectly correlated or uncorrelated (i.e., $r = 1.0$ or $r = 0.0$, respectively) across all stimuli, all stimuli will fall on a single point. Three clusters were identifiable in the MDS plot, one containing all of the grating stimuli (*red cluster*), another containing 17 large angles and intersections (*green cluster*), and a third (*blue cluster*) containing the remaining contour stimuli. These clusters were highly significant as measured by the *D* ratio test (where the *D* ratio is a direct analog of the *F* ratio; see METHODS), with 0/1,000 rounds passing the criterion, indicating that the underlying correlation patterns were highly nonrandom. The pattern in Fig. 8*D* is very similar to those in a previous analysis of the same data set (Hegdé and Van Essen 2003) that used a somewhat broader

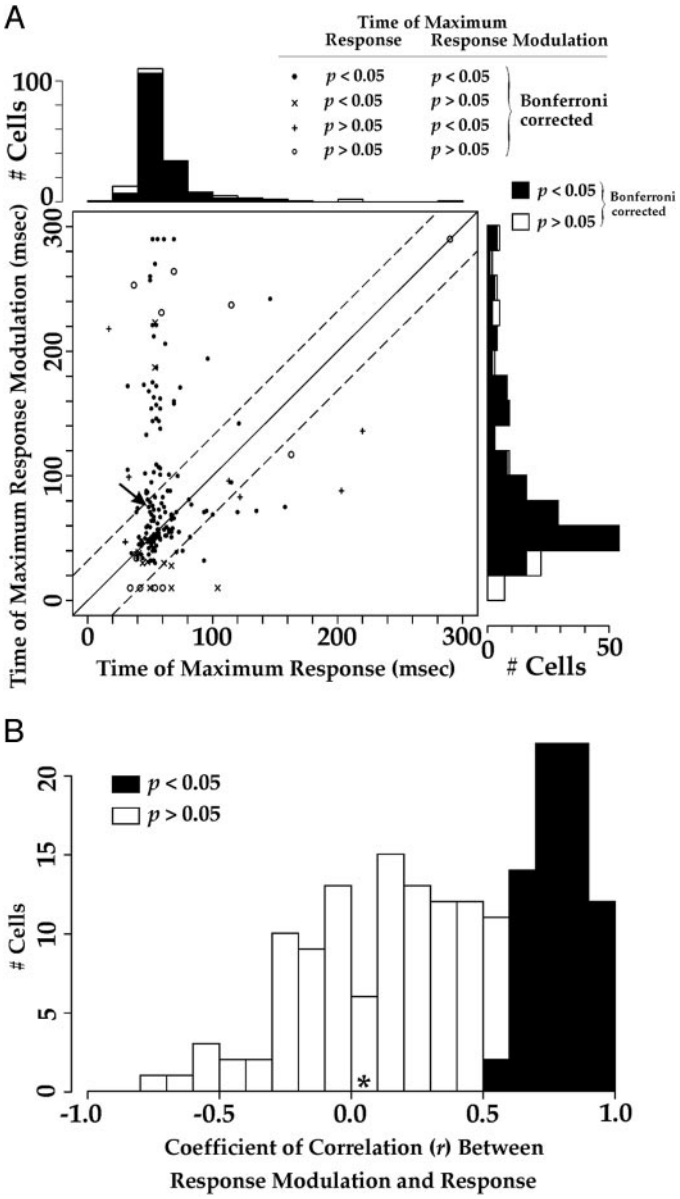

FIG. 7. Relationship between the time of maximum response vs. the time of maximum response modulation. For each cell, the time of peak firing rate and time of peak response modulation were calculated to the nearest millisecond, and the statistical significance of the peaks determined, as described in METHODS. Resulting values are plotted in the *scatterplot* according to whether one or both values were statistically significant (*inset*). Diagonal represents the iso-time line. Dashed lines denote a time interval of ±20 ms from the iso-time line. Histograms on either axis denote the bin distribution of the corresponding time points. *B*: correlation between firing rate and response modulation. Coefficient of correlation (*r*) between the firing rate vs. the RMI values across all 15 bins was calculated for each cell. Distribution of *r* values for all V2 cells is shown here in histogram form. Exemplar cell in Fig. 2 is denoted by an arrow in *A* and by an asterisk in *B*.

time window for analysis (36–134 ms [mean]). The distinction between gratings and contours clearly underlay the separation of the *red* cluster from the other 2 (*green and blue*) clusters, whereas the selectivity for stimulus size and for specific angles and curved stimuli may underlie the differentiation between the 2 (*blue* vs. *green*) contour clusters (see Hegdé and Van Essen 2003). For later bins, the clustering of stimuli was progressively less pronounced, although still discernible in both the MDS plot (Fig. 8*E* for the 280–300 ms window) and the correlation matrix (Fig. 8*B*, *panels 3* and *4*), indicating that the population response was substantially but not completely decorrelated after this point.

To assess the complexity of the population response during each bin, we analyzed each correlation matrix using PCA (see METHODS). The proportion of the data accounted for by the most informative principal components, and the number of principal components required to account for a criterion amount of the data, are 2 measures of the dimensionality, or complexity, of the data (see Kachigan 1991, p. 246–247). If the population response during a given bin were perfectly decorrelated, each principal component would be expected to account for 0.78% of the total response variation (given a set of 128 stimuli). Figure 9 shows the 10 most informative principal components for each of the 15 bins. During the 0–20 ms bin, before the response onset, the first 10 principal components together account for only 46% of the variance. During the 40–60 ms bin, when the population is maximally correlated (see Fig. 8, *B–D*), the first principal component by itself accounts for 46% of the variance, and the top 3, 5, and 10 components together accounted for 78, 85, and 92% of the data, respectively. Thus a relatively small number of response dimensions accounted for most of the population response during the early transient response. The complexity of the of the population response increased markedly between 60 and 160 ms; between 160 and 300 ms, the first principal component accounted for 13–18% of the variance and the first 10 components accounted for 58–62% of the variance. We obtained qualitatively similar results when these analyses were repeated using bins with equal spike counts, described above (data not shown).

Together, these results indicate the population response was relatively correlated, or low-dimensional, early in the response, and significantly decorrelated (increased in dimensionality) in the period between 60 and 160 ms after stimulus onset.

Temporal changes in the response profiles of individual V2 cells

The decorrelations of the population response described above might in principle result from a decorrelation of the response profile of a subset of cells, or from a widespread decorrelation across the population. To distinguish between the 2 scenarios, we measured the extent to which the response profiles of individual cells changed over time. To do this, we calculated the correlation coefficient *r* between the given cell's response during a given pair of bins for each pairwise combination of the 15 bins (see METHODS).

Figure 10*A* illustrates the changes in the response profile of the exemplar cell over the course of the response relative to its response profiles during each of the 4 earliest bins. The thick solid line shows the *r* values across all bins measured relative to the 20–40 ms bin, the earliest bin during which the cell's responses were both significantly elevated from background levels and were significantly modulated (see Fig. 6*A*). The *r* value during the next bin (40–60 ms bin) was 0.20, indicating that the response profiles decorrelated substantially between the 2 bins. In the subsequent bins, the *r* values stabilized at a lower level (range, 0.06–0.17), slightly above the chance level (horizontal arrow on the *y*-axis). Similar results were obtained when the correlation coefficients were calculated relative to the

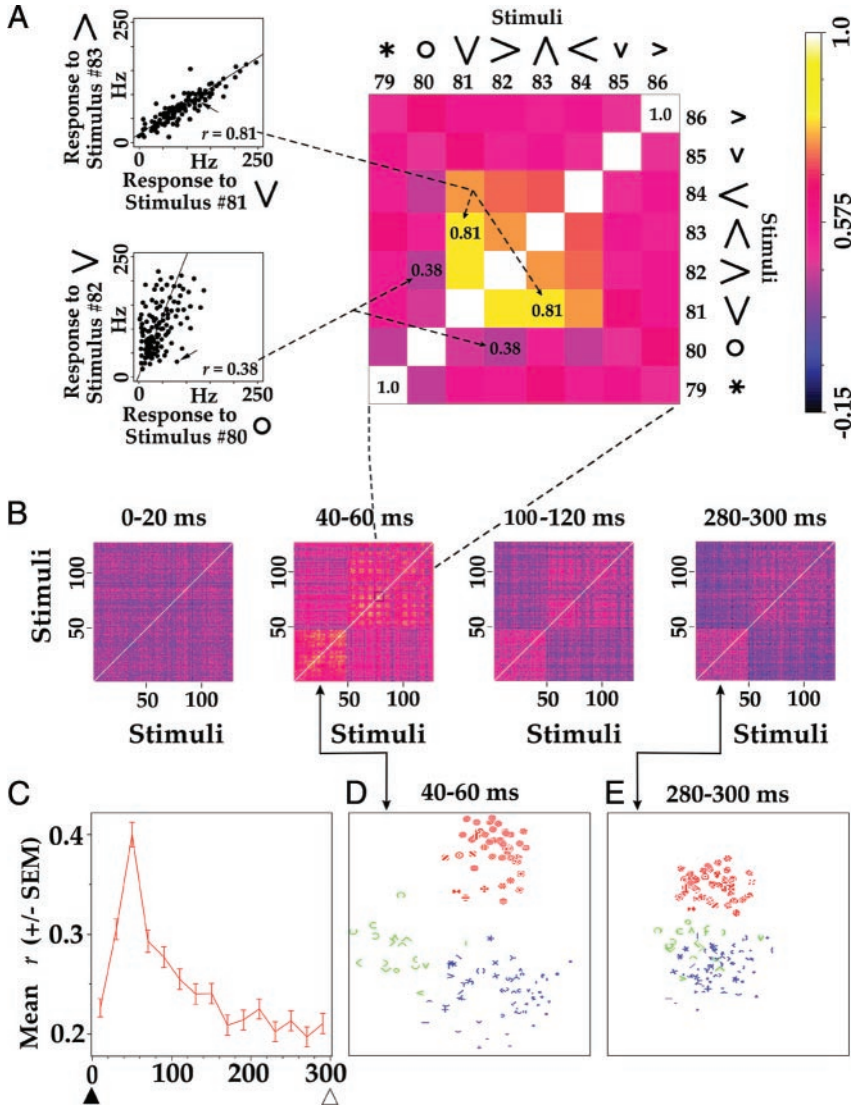

FIG. 8. Temporal dynamics of the population response. *A*: construction of the correlation matrix used in the population analyses. Each panel on *left* shows the responses of V2 neurons (dots) to a selected pair of stimuli during the 40- to 60-ms bin plotted against each other. In either panel, the arrow denotes the responses of the exemplar cell in Fig. 2, and the line denotes the best-fitting regression line. Correlation coefficient r is a measure of the deviation of the responses from this regression line. *Right panel*: magnified portion of the correlation matrix for the 40- to 60-ms bin plotted according to the color scale at *far right*. *Icons* denote the relevant stimuli, oriented and numbered as in Fig. 1. To construct the correlation matrix for a given time bin, the r value from each possible pair of stimuli was calculated and assigned to the corresponding element of the correlation matrix (dashed arrows). Elements along the diagonal from *bottom left* to *top right* represent the correlation of the responses to a given stimulus with themselves ($r = 1.0$). Note that the matrix is symmetric about this diagonal, given that $r(i, j) \equiv r(j, i)$ for any 2 stimuli i and j. *B*: correlation matrices for 4 selected bins, each plotted according to the color scale in *A*. *C*: average r value ($\pm$SE) during the different bins. *D* and *E*: MDS plots of the correlation matrix during 2 selected bins (double-headed arrows), both drawn to the same scale. Three clusters of stimuli delineated by the MDS are highlighted using arbitrary colors: *red*, *green*, and *blue*.

40–60 ms bin (thick dashed line) or to the 60–80-ms bin (thin dotted line), except that the average r values stabilized at a higher level (mean $r = 0.18$).

Figure 10*B* illustrates the average change in the response profiles ($\pm$ cell-to-cell SE) for all V2 cells. These results were qualitatively similar to those for the exemplar cell, except that the magnitude of decorrelation over the course of the response was somewhat less pronounced. Note that the SE of the r values (error bars) changed little over time (range, 0.031–0.036), suggesting that the decorrelation of the response was

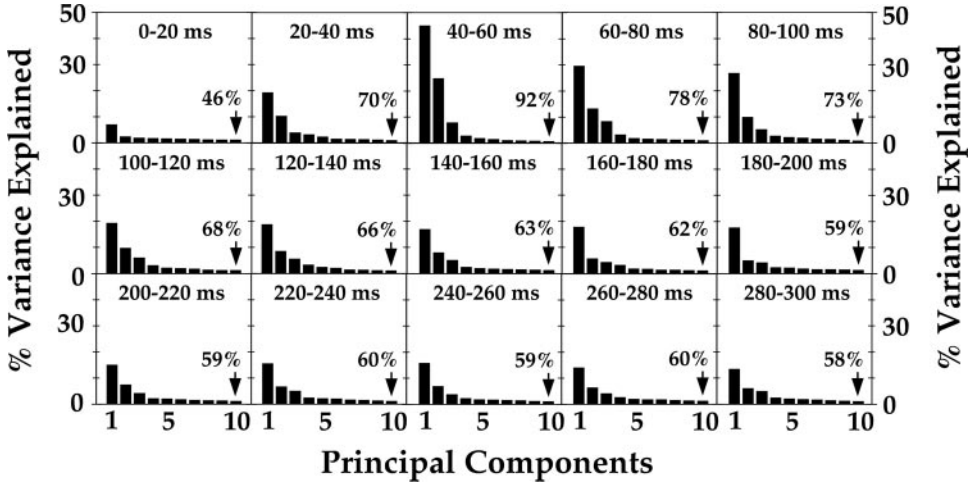

FIG. 9. Principal components analysis (PCA) of the population response. Correlation matrix for each bin was analyzed using PCA. Proportion of the data in the given correlation matrix accounted for the 10 most influential principal components is shown here for each bin. For each bin, the total variance in the data accounted for by the top 10 components together is denoted by the arrow.

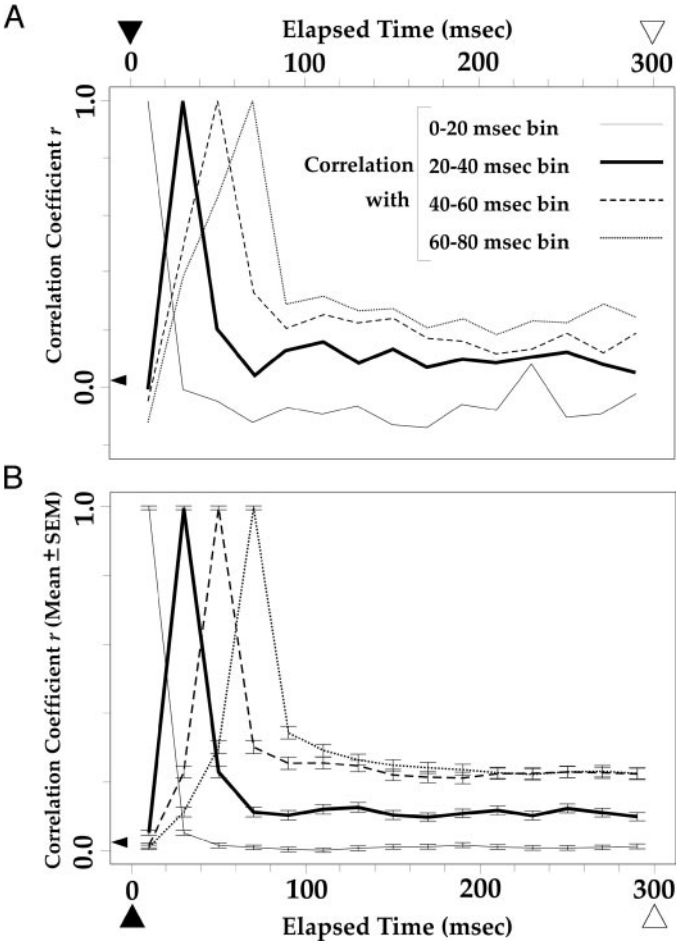

FIG. 10. Temporal changes in the shape selectivity profile of individual cells. Shape-selectivity profile of each cell during a given bin was compared with its shape selectivity profile during each of the other bins using correlation coefficient *r*. This process was repeated for each of the 180 cells for each of the 15 bins. This plot shows the *r* values relative to the 4 consecutive bins spanning 0–80 ms. *A*: *r* values for the exemplar cell in Fig. 2. *B*: average *r* values (± cell-to-cell SE) for all 180 cells. In either panel, the thick solid line denotes the average correlation between the cells' responses during the 20- to 40-ms bin with the responses during each of the other bins, along with correlation with itself (average *r* value of 1.0 ± 0.0; *top*); the other 2 lines show similar measurements relative to the 40- to 60-ms bin (thick dashed line), and 60–80 ms (thin dotted line). Arrowheads on the *y*-axis denotes the average randomized *r* value from $4 \times 15 \times 10^3$ rounds of randomization of the responses of the exemplar cell (*A*) or all cells. Note that the *y*-axis scales for the 2 panels are slightly different.

widespread across V2 cells. If the decorrelation were attributable to the changes in the response profiles of a small subset of cells while the response profiles of the remaining cells stayed largely unchanged, the cell-to-cell variation of the *r* values would be expected to increase with decreasing mean *r* values.

The nature of the temporal changes in shape profiles were diverse; we found no clear patterns across subpopulations of cells in this regard. That is, given the response profile of an individual cell during the early part of the response, it was not possible to predict, with any accuracy, how the response profile of the cell might change later in the response, other than the trend toward decorrelation already discussed.

DISCUSSION

The central finding of this study is that the shape information conveyed by V2 cells changes significantly over the time course of responses to static visual stimuli presented within the classical receptive field. This was evident in each of several measures, including sharpness of tuning (Fig. 4*D*), signal-to-noise measures (Fig. 5), response profiles of individual cells (Fig. 10), and stimulus-related correlations across the neuronal population (Figs. 8 and 9). We also find that for many V2 cells, the signal-to-noise ratio peaks relatively early in the response (although often later than the peak in the firing rate itself), and generally lower but statistically significant for the remainder of the response (Figs. 6 and 7).

As noted in the INTRODUCTION, many previous studies have addressed the temporal dynamics of various response metrics used in other visual areas or sensory systems. In the visual system, LGN (lateral geniculate nucleus) neurons temporally decorrelate in response to natural movies, but not to white noise, by a process involving linear temporal filtering characteristics of neurons (Dan et al. 1996). In the visual cortex, many previous studies have explored the temporal dynamics of individual cell responses, especially in area V1 (see, e.g., Albrecht et al. 2002; Bredfeldt and Ringach 2002; Celebrini et al. 1993; DeAngelis et al. 1993; Jones and Palmer 1987; Mazer et al. 2002; Menz and Freeman 2003, 2004; Müller et al. 2001; Ringach et al. 1997; Shapley et al. 2003) and in the inferior temporal cortex (Edwards et al. 2003; Keysers et al. 2001; Oram and Perrett 1992; Tovée et al. 1993). Recently, Müller et al. (2001) analyzed the temporal dynamics of the signal-to-noise ratio in area V1 of the anesthetized monkey and found that V1 cells convey much more information during the initial transients than during later periods of the same duration. They reported time-dependent changes in the contrast response function but not in orientation tuning curves, and they found that orientation tuning estimated from the first 150 ms of response was indistinguishable from that estimated over the first 1,250 ms. In contrast, Zohary et al. (1990) reported increased orientation discriminability as the integration window increased from 60–100 ms, and Ringach et al. (1997) reported significant time dependency of orientation tuning using a finer-grained temporal analysis (10 vs. 50 ms bins). In the domain of stereopsis, Menz and Freeman (2003, 2004) showed that binocular disparity tuning in cat visual cortex sharpens with time, consistent with coarse-to-fine processing.

In the olfactory system, it has been recently reported that the population response of zebrafish mitral cells to odors decorrelates over a period of 1 s or so (Friedrich and Laurent 2001, 2004). This is qualitatively analogous to our observations, except that it occurs over a much slower time course (~800 ms) and is not associated with an increased sharpness of tuning.

An interesting possibility is that the broadly tuned transient responses of V2 neurons provide a relatively low-dimensional representation that subserves a rapid, relatively coarse-grained initial shape analysis (e.g., predator or not?), whereas the more sharply tuned sustained responses provide a higher-dimensional representation that subserves finer-grained discriminative capacities (e.g., which prey is better?) (see Churchland et al. 1994; Field 1995; Friedrich and Laurent 2001; Roweis and Saul 2000; Seung and Lee 2000; Tennenbaum et al. 2000; also see Edwards et al. 2003, and references therein).

Many lines of psychophysical evidence support the notion that coarse-grained object recognition can occur on a faster timescale, whereas finer-grained object recognition is slower

(Donders 1969; Luce 1986; Posner 1978). Reaction times and processing times tend to be shorter for simple detection or categorization tasks than for discrimination tasks (Fabre-Thorpe et al. 1998; Liu et al. 2002; Luce 1986; Posner 1978; also see Treisman 1988). In addition, when visual stimuli are flashed only briefly, followed by a mask or as part of a continuous image sequence, subjects can often accurately detect the presence of a given visual object, but not the precise features of the object (Fabre-Thorpe et al. 1998; Fize et al. 2000; Keysers et al. 2001; Reynolds 1981; Thorpe et al. 1996).

Neural mechanisms of response decorrelation

What aspects of neural circuitry might account for the changes in sharpness of tuning and the progressive decorrelation across the neuronal population? Saturation of responses during the initial transient could be one contributing factor, but our analysis of response variance relative to the mean suggests that the relative refractory period is not the main factor. However, there might be alternative forms of saturation (e.g., involving contrast normalization mechanisms) that are consistent with our data.

A response decay after an initial transient can arise from depression of cortical excitatory synapses (Markram and Tsodyks 1996; Müller et al. 2001; Varela et al. 1997). However, the fact that V2 responses decorrelate while they decrease in magnitude suggests that the decay is not simply a function of generalized, nonspecific synaptic depression. Response decorrelations in visual cortex may also arise from recruitment of intracortical inputs that shape classical receptive field responses, from context-dependent effects outside the classical receptive field (see Vinje and Gallant 2000), or as a function of recent stimulation of the receptive field (see Müller et al. 1999; also see Nelson 1991).

Time as a coding dimension

Given that the shape of tuning profiles of V2 neurons can vary over time, it is obviously of interest to know whether the processes used to decode this information in other visual areas must take these characteristics into account. The notion that the temporal pattern of sensory responses is used to code meaningful information has been suggested by others for the visual system (McClurkin et al. 1991; Richmond and Optican 1990) and the olfactory system (Friedrich and Laurent 2001). This notion of temporal structure in mean firing rates is distinct from temporal coding hypotheses based on synchronized firing among subsets of neurons (for reviews, see Gray 1999; Salinas and Sejnowski 2001; Usrey and Reid 1999). However, both types of temporal coding, though intriguing, remain controversial (Averbeck and Lee 2004; Shadlen and Movshon 1999) and are difficult to test incisively.

ACKNOWLEDGMENTS

We thank G. DeAngelis, B. Olshausen, B. Krekelberg, and P. Tiesinga for valuable discussions and comments and S. Danker for assistance with manuscript preparation.

Present address of J. Hegdé: Vision Center Laboratory, The Salk Institute for Biological Studies, 10010 N. Torrey Pines Rd., La Jolla, CA 92037.

GRANTS

This work was supported by National Eye Institute Grant EY-02091.

REFERENCES

Abbott LF. Decoding neuronal firing and modelling neural networks. *Q Rev Biophys* 27: 291–331, 1994.

Adrian ED. The impulses produced by sensory nerve endings. Part I. *J Physiol* 61: 49–72, 1926.

Albrecht DG, Geisler WS, Frazor RA, and Crane AM. Visual cortex neurons of monkeys and cats: temporal dynamics of the contrast response function. *J Neurophysiol* 88: 888–913, 2002.

Averbeck BB and Lee D. Coding and transmission of information by neural ensembles. *Trends Neurosci* 27: 225–230, 2004.

Bergen JR. Theories of visual texture perception. In: *Vision and Visual Dysfunction*, edited by Regan D. New York: Macmillan, 1991, vol. 10B, p. 114–134.

Brase CH and Brase CP. *Understandable Statistics.* Lexington, MA: DC Heath and Co., 1995.

Bredfeldt CE and Ringach DL. Dynamics of spatial frequency tuning in macaque V1. *J Neurosci* 22: 1976–1984, 2002.

Celebrini S, Thorpe S, Trotter Y, and Imbert M. Dynamics of orientation coding in area V1 of the awake primate. *Vis Neurosci* 10: 811–825, 1993.

Chee-Orts MN and Optican LM. Cluster method for analysis of transmitted information in multivariate neuronal data. *Biol Cybern* 69: 29–35, 1993.

Churchland PS, Ramachandran VS, and Sejnowski TJ. A critique of pure vision. In: *Large-Scale Neuronal Theories of the Brain*, edited by Koch C and Davis JL. Cambridge, MA: MIT Press, 1994, p. 23–60.

Cook EP and Maunsell JH. Dynamics of neuronal responses in macaque MT and VIP during motion detection. *Nat Neurosci* 5: 985–994, 2002.

Dan Y, Atick JJ, and Reid RC. Efficient coding of natural scenes in the lateral geniculate nucleus: experimental test of a computational theory. *J Neurosci* 16: 3351–3362, 1996.

DeAngelis GC, Ohzawa I, and Freeman RD. Spatiotemporal organization of simple-cell receptive fields in the cat's striate cortex. I. General characteristics and postnatal development. *J Neurophysiol* 69: 1091–1117, 1993.

Donders FC. On the speed of mental processes. *Acta Psychol* (*Amst.*) 30: 412–431, 1969.

Duffy CJ and Wurtz RH. Multiple temporal components of optic flow responses in MST neurons. *Exp Brain Res* 114: 472–482, 1997.

Eagleson R. Measurement of the 2D affine Lie group parameters for visual motion analysis. *Spat Vis* 6: 183–198, 1992.

Edgington ES. *Randomization Tests.* New York: Marcel Dekker, 1995.

Edwards R, Xiao D, Keysers C, Földiák P, and Perrett D. Color sensitivity of cells responsive to complex stimuli in the temporal cortex. *J Neurophysiol* 90: 1245–1256, 2003.

Fabre-Thorpe M, Richard G, and Thorpe SJ. Rapid categorization of natural images by rhesus monkeys. *Neuroreport* 9: 303–308, 1998.

Field D J. Visual coding, redundancy and "feature detection." In: *The Handbook of Brain Theory and Neural Networks*, edited by Arbib M. Cambridge, MA: MIT Press, 1995, p. 1012–1016.

Fize D, Boulanouar K, Chatel Y, Ranjeva J-P, Fabre-Thorpe M, and Thorpe SJ. Brain areas involved in rapid categorization of natural images: an event-related fMRI study. *Neuroimage* 11: 634–643, 2000.

Frazor RA, Albrecht DG, Geisler WS, and Crane AM. Temporal dynamics of the spatial frequency response function. *J Neurophysiol* [Epub ahead of print] 2004.

Friedrich RW and Laurent G. Dynamic optimization of odor representations by slow temporal patterning of mitral cell activity. *Science* 291: 889–894, 2001.

Friedrich RW and Laurent G. Dynamics of olfactory bulb input and output activity during odor stimulation in zebrafish. *J Neurophysiol* [Epub ahead of print] 2004.

Gallant JL, Connor CE, Rakshit S, Lewis JW, and Van Essen DC. Neural responses to polar, hyperbolic, and Cartesian gratings in area V4 of the macaque monkey. *J Neurophysiol* 76: 2718–2739, 1996.

Geisler WS, Perry JS, Super BJ, and Galogly DP. Edge co-occurence in natural images predicts contour grouping performance. *Vision Res* 41: 711–724, 2001.

Geisler WS and Super BJ. Perceptual organization of two-dimensional patterns. *Psychol Rev* 107: 677–708, 2000.

Gray CM. The temporal correlation hypothesis of visual feature integration: still alive and well. *Neuron* 24: 31–47, 1999.

Hegdé J and Van Essen DC. Selectivity for complex shapes in primate visual area V2. *J Neurosci* 20: RC61–RC66, 2000.

Hegdé J and Van Essen DC. Strategies of shape representation in macaque visual area V2. Selectivity for complex shapes in primate visual area V2. *Vis Neurosci* 20: 313–328, 2003.

Huberty CJ and Morris JD. Multivariate analysis versus multiple univariate analyses. *Psychol Bull* 105: 302–308, 1989.

Jones JP and Palmer LA. The two-dimensional spatial structure of simple receptive fields in cat striate cortex. *J Neurophysiol* 58: 1187–1211, 1987.

Kachigan SK. *Multivariate Statistical Analysis.* New York: Radius Press, 1991.

Keysers C, Xiao DK, Földiák P, and Perrett DI. The speed of sight. *J Cogn Neurosci* 13: 90–101, 2001.

Knierim JJ and Van Essen DC. Neuronal responses to static texture patterns in area V1 of the alert macaque monkey. *J Neurophysiol* 67: 961–980, 1992.

Lamme VA, Rodriguez-Rodriguez V, and Spekreijse H. Separate processing dynamics for texture elements, boundaries and surfaces in primary visual cortex of the macaque monkey. *Cereb Cortex* 9: 406–413, 1999.

Lee TS and Nguyen M. Dynamics of subjective contour formation in the early visual cortex. *Proc Natl Acad Sci USA* 98: 1907–1911, 2001.

Lisberger SG and Movshon JA. Visual motion analysis for pursuit eye movements in area MT of macaque monkeys. *J Neurosci* 19: 2224–2246, 1999.

Liu J, Harris A, and Kanwisher N. Stages of processing in face perception: an MEG study. *Nat Neurosci* 5: 910–916, 2002.

Luce RD. *Response Times*: *Their Role in Inferring Elementary Operations.* Oxford, UK: Oxford Univ. Press, 1986.

Manly BFJ. *Randomization and Monte-Carlo Methods in Biology.* New York: Chapman & Hall, 1991.

Markram H and Tsodyks M. Redistribution of synaptic efficacy between neocortical pyramidal neurons. *Nature* 382: 807–810, 1996.

Mazer JA, Vinje VE, McDermott J, Schiller PH, and Gallant JL. Spatial frequency and orientation tuning dynamics in area V1. *Proc Natl Acad Sci USA* 99: 1645–1650, 2002.

McAdams CJ and Maunsell JHR. Effects of attention on the reliability of individual neurons in monkey visual cortex. *Neuron* 23: 765–773, 1999.

McClurkin JW, Optican LM, Richmond BJ, and Gawne TJ. Concurrent processing and complexity of temporally encoded neuronal messages in visual perception. *Science* 25: 675–677, 1991.

Menz MD and Freeman RD. Stereoscopic depth processing in the visual cortex: a coarse-to-fine mechanism. *Nat Neurosci* 6: 59–65, 2003.

Menz MD and Freeman RD. Temporal dynamics of binocular disparity processing in the central visual pathway. *J Neurophysiol* 91: 1782–1793, 2004.

Müller JR, Metha AB, Krauskopf J, and Lennie P. Rapid adaptation in visual cortex to the structure of images. *Science* 285: 1405–1408, 1999.

Müller JR, Metha AB, Krauskopf J, and Lennie P. Information conveyed by onset transients in responses of striate cortical neurons. *J Neurosci* 21: 6978–6990, 2001.

Nelson SB. Temporal interactions in the cat visual system. I. Orientation-selective suppression in the visual cortex. *J Neurosci* 11: 344–356, 1991.

Oram MW and Perrett DI. Time course of neural responses discriminating different views of the face and head. *J Neurophysiol* 68: 70–84, 1992.

Pack CC and Born RT. Temporal dynamics of a neural solution to the aperture problem in visual area MT of macaque brain. *Nature* 409: 1040–1042, 2001.

Panzeri S. *Quantitative Methods for Analyzing Information Processing in the Mammalian Cortex* (PhD thesis). Trieste, Italy: International School for Advanced Studies, 1996.

Panzeri S and Treves A. Analytical estimates of limited sampling biases in different information measures. *Netw Comput Neural Syst* 7: 87–107, 1996.

Perona P. Deformable kernels in early vision. *IEEE Conf Vision Pattern Recognit* 761: 222–227, 1991.

Posner MI. *Chronometric Explorations of Mind.* Hillsdale, NJ: Erlbaum, 1978.

Pouget A, Dayan P, and Zemel R. Information processing with population codes. *Nat Rev Neurosci* 1: 125–132, 2000.

Reynolds RI. Perception of an illusory contour as a function of processing time. *Perception* 10: 107–115, 1981.

Richmond BJ and Optican LM. Temporal encoding of two-dimensional patterns by single units in primate visual cortex. II. Information transmission. *J Neurophysiol* 64: 370–380, 1990.

Rieke F, Warland D, de Ruyter van Steveninck R, and Bialek W. *Spikes.* Cambridge, MA: MIT Press, 1998.

Ringach DL, Hawken MJ, and Shapley R. Dynamics of orientation tuning in macaque primary visual cortex. *Nature* 387: 281–284, 1997.

Rogers-Ramachandran DC and Ramachandran VS. Psychophysical evidence for boundary and surface systems in human vision. *Vision Res* 38: 71–77, 1997.

Rolls ET, Franco L, Aggelopoulos NC, and Reece S. An information theoretic approach to the contributions of the firing rates and the correlations between the firing of neurons. *J Neurophysiol* 89: 2810–2822, 2003.

Roweis ST and Saul LK. Nonlinear dimensionality reduction by locally linear embedding. *Science* 290: 2323–2326, 2000.

Salinas E and Sejnowski TJ. Correlated neuronal activity and the flow of neural information. *Nat Rev Neurosci* 2: 539–550, 2001.

Savitz DA and Olshan AF. Multiple comparisons and related issues in the interpretation of epidemiological data. *Am J Epidemiol* 142: 904–908, 1995.

Seung HS and Lee DD. The manifold ways of perception. *Science* 290: 2268–2269, 2000.

Shadlen MN and Movshon JA. Synchrony unbound: a critical evaluation of the temporal binding hypothesis. *Neuron* 24: 67–77, 111–125, 1999.

Shadlen MN and Newsome WT. The variable discharge of cortical neurons: implications for connectivity, computation, and information coding. *J Neurosci* 18: 3870–3896, 1998.

Shadlen MN and Newsome WT. Noise, neural codes and cortical organization. *Curr Opin Neurobiol* 4: 569–579, 1994.

Shapley R, Hawken M, and Ringach DL. Dynamics of orientation selectivity in the primary visual cortex and the importance of cortical inhibition. *Neuron* 38: 689–699, 2003.

Sigman M, Cecchi GA, Gilbert CD, and Magnasco MO. On a common circle: natural scenes and Gestalt rules. *Proc Natl Acad Sci USA* 98: 1935–1940, 2001.

Sneath PH and Sokal RR. *Numerical Taxonomy.* San Francisco, CA: Freeman, 1973.

Softky WR and Koch C. The highly irregular firing of cortical cells is inconsistent with temporal integration of random EPSPs. *J Neurosci* 13: 334–350, 1993.

Sokal RR and Rohlf FJ. The comparison of dendrograms by objective methods. *Taxon* 11: 33–40, 1962.

Tenenbaum JB, de Silva V, and Langford JC. A global geometric framework for nonlinear dimensionality reduction. *Science* 290: 2319–2323, 2000.

Thompson JR. Multiple comparisons and related issues in the interpretation of epidemiological data [Invited commentary]. *Am J Epidemiol* 147: 801–806, 1998.

Thorpe S, Fize D, and Marlot C. Speed of processing in the human visual system. *Nature* 381: 520–522, 1996.

Tolhurst DJ, Movshon JA, and Dean AF. The statistical reliability of signals in single neurons in cat and monkey visual cortex. *Vision Res* 23: 775–785, 1983.

Tolhurst DJ, Walker NS, Thompson ID, and Dean AF. Non-linearities of temporal summation in neurones in area 17 of the cat. *Exp Brain Res* 38: 431–435, 1980.

Tovée MJ, Rolls ET, Treves A, and Bellis RP. Information encoding and the responses of single neurons in the primate temporal visual cortex. *J Neurophysiol* 70: 640–654, 1993.

Treisman A. Features and objects: the fourteenth Bartlett memorial lecture. *Q J Exp Psychol A* 40: 201–237, 1988.

Usrey W and Reid RC. Synchronous activity in the visual system. *Annu Rev Physiol* 61: 435–456, 1999.

Varela JA, Sen K, Gibson J, Frost J, Abbott LF, and Nelson SB. A quantitative description of short-term plasticity at excitatory synapses in layer 2/3 of rat primary visual cortex. *J Neurosci* 17: 7926–7940, 1997.

Wiener MC, Oram MW, Liu Z, and Richmond BJ. Consistency of encoding in monkey visual cortex. *J Neurosci* 21: 8210–8221, 2001.

Wilkinson F, Wilson HR, and Habak C. Detection and recognition of radial frequency patterns. *Vision Res* 38: 3555–3568, 1998.

Zhou H, Friedman HS, and von der Heydt R. Coding of border ownership in monkey visual cortex. *J Neurosci* 20: 6594–6611, 2000.

Zohary E, Hillman P, and Hochstein S. Time course of perceptual discrimination and single neuron reliability. *Biol Cybern* 62: 475–486, 1990.